



Cite this: *Catal. Sci. Technol.*, 2015,
5, 296

On the role of H₂ to modify surface NO_x species over Ag–Al₂O₃ as lean NO_x reduction catalyst: TPD and DRIFTS studies

Muhammad Mufti Azis,^{ab} Hanna Härelind^b and Derek Creaser^{*a}

Formation and stability of surface NO_x species related to the promotional effect of H₂ over Ag–Al₂O₃ as NO_x reduction catalyst were investigated with temperature-programmed desorption and DRIFT spectroscopy. Formation of two groups of surface NO_x species was found: a less thermally stable group of “low temperature (LT) species” and a more thermally stable group of “high temperature (HT) species”. The LT NO_x was attributable to the decomposition of surface NO_x species formed on the active sites where its elimination by addition of H₂ or thermal decomposition correlated with higher NO oxidation and NO_x reduction conversion. Under reaction conditions, these possibly inhibiting LT NO_x species were stable up to about 300 °C and their formation depended on donation of oxygen from surface oxides. Removal of LT nitrate species by H₂ accounted for only a fraction of the increased NO oxidation and NO_x reduction conversion by co-feeding H₂. Furthermore, it was also found that H₂ facilitates formation of HT NO_x that primarily corresponded to the decomposition of spectator species on the Al₂O₃ support identified as monodentate nitrate species. From TPD studies of C₃H₆–SCR, it was shown that H₂ not only eliminated LT NO_x but also promoted formation of greater quantities of adsorbed hydrocarbons.

Received 24th June 2014,
Accepted 20th August 2014

DOI: 10.1039/c4cy00816b

www.rsc.org/catalysis

Introduction

With a growing demand to reduce fuel consumption, lean-burn and diesel engine vehicles will continue to comprise an increasing fraction of road-vehicles in the future. The regulation of NO_x (NO + NO₂) emissions from the transportation sector in the upcoming years will be more stringent and therefore it is urgently required to develop efficient and reliable NO_x reduction after treatment systems for a wide variety of lean-burn or diesel engines. Selective catalytic reduction (SCR) of NO_x with hydrocarbons (HC) has remained as one possible concept to catalytically reduce NO_x emissions from lean-burn and diesel engine vehicles. For hydrocarbon-selective catalytic reduction (HC-SCR), Ag/Al₂O₃ catalysts have been considered to have potential due to their lower cost, higher tolerance towards water vapor and sulfur^{1,2} but also lower selectivity to N₂O formation compared to PGM catalysts.³

However, it is important to mention that Ag/Al₂O₃ exhibits poor NO_x reduction activity in the lower temperature region. Below 400 °C, the NO_x reduction activity decreases abruptly

which has been considered to be due to self-inhibition by adsorbed nitrates on the active sites of the catalyst.⁴ It has been shown that addition of H₂ can drastically promote NO_x reduction activity in the lower temperature region.⁵ The so called “H₂-effect” results in better NO_x reduction activity and a wider temperature operating window. Nevertheless, the reaction mechanism of HC-SCR over Ag/Al₂O₃ remains a challenging issue since it involves a number of reaction intermediates and surface species during the reaction. As a result, the mechanisms by which H₂ promotes NO_x reduction with Ag/Al₂O₃ are not entirely identified.

Generally, the reaction mechanism of HC-SCR over Ag/Al₂O₃ is initiated by activation of NO_x and HC. Activation of NO_x is characterized by formation of surface NO_x species mainly as nitrate and/or nitrite species. Subsequently, oxygen partially oxidizes hydrocarbons (HC activation) to form oxygenated HC surface species which react further with surface NO_x species and eventually lead to the formation of N₂. For this reason, surface NO_x species have been suggested to be important intermediates and therefore it is important to understand their formation, stability, reactivity and possible inhibition effects to elucidate the mechanism of HC-SCR.

Temperature-programmed desorption (TPD) is a useful technique to investigate the thermal stability of adsorbed species. TPD studies to investigate the stability of surface NO_x species over Ag/Al₂O₃ have been reported in the literature.^{6–9} Following adsorption of NO and O₂ over

^a Division of Chemical Engineering, Department of Chemical and Biological Engineering, Chalmers University of Technology, Göteborg, Sweden SE-41296.
E-mail: derek.creaser@chalmers.se; Fax: +4631 7723035; Tel: +4631 7723023

^b Competence Centre for Catalysis (KCK), Department of Chemical and Biological Engineering, Chalmers University of Technology, Göteborg, Sweden SE-41296



Ag/Al₂O₃, two NO_x desorption peaks at low temperature (250–340 °C) and high temperature (435–539°) have been reported.^{6,9} Several attempts were made to identify the origin of these NO_x desorption peaks. By combining TPD and IR spectroscopy, Kameoka *et al.*⁶ found that the peaks originated from three types of surface nitrates *i.e.* bridging, bidentate and monodentate nitrates. From additional TPD studies,^{7–9} it was pointed out that NO_x desorption peaks at high temperature (~440 °C (ref. 7 and 8) and 539 °C (ref. 9)) resulted from surface nitrate decomposition.

It is interesting to note that H₂ may play a dual role in its interaction with nitrate species. On one hand, H₂ has been proposed to promote elimination of nitrates during H₂-assisted HC-SCR.^{10–16} On the other hand, it has also been shown that H₂ activates accumulation of nitrates on the surface, especially during NO oxidation.^{8,10,17–19}

Elimination of surface nitrates from the active silver species by H₂ has been proposed as one probable key step in the “H₂-effect” for low temperature HC-SCR.^{10–16} H₂ has also been found to promote NO oxidation^{8,13,17,18,20} and our previous study has simulated H₂-assisted NO oxidation based on the main role of H₂ to eliminate poisonous surface nitrate species.²¹ It is important to mention, however, that H₂ has been proposed to have several other roles in HC-SCR which have been discussed in the literature such as to facilitate modification of surface species and active Ag sites.^{5,10,12,13,16,22,23}

Seemingly contradictory to hydrogen's proposed role to eliminate nitrates during HC-SCR, *in situ* FTIR studies have been widely presented in the literature showing that H₂ plays an important role to activate the accumulation of surface nitrates following exposure of the catalyst to a NO–O₂–H₂ gas mixture.^{10,17–19} Recently, Kim *et al.*²³ also suggested that the kinetic effects of H₂ was to promote formation of surface nitrate that later reacts with adsorbed HC. With the low silver loadings that are common for Ag/Al₂O₃ catalysts, it is also reasonable to expect that alumina also facilitates adsorption of surface NO_x species. In addition, the existence of both silver nitrate and aluminium nitrate and their interaction following NO_x adsorption has been proposed.^{8,11,24} Unfortunately, *in situ* IR analysis indicates overlapping peaks for nitrates over Ag/Al₂O₃ and bare Al₂O₃ which makes it difficult to discriminate between nitrates on the Al₂O₃ support and silver particles.^{17,25,26}

In the present work, a series of TPD studies of NO_x were carried out over Ag–Al₂O₃ and Al₂O₃ catalysts to quantify and characterize the stability of surface NO_x species related to Ag–Al₂O₃ as a HC-SCR catalyst. In addition, *in situ* DRIFT spectroscopy experiments were also carried out to characterize formation of adsorbed NO_x species. This study has also aimed to demonstrate the effect of H₂ to modify the quantities and position of surface NO_x species. These effects will also be correlated to the activity of the catalyst for NO oxidation and C₃H₆-SCR to determine quantitatively to what extent H₂ removal of inhibiting nitrates may contribute to the so called “H₂-effect”. An additional objective for studying

surface NO_x species was to examine whether these apparently contradictory roles for H₂, discussed above, could be compatible. We have focused our work on the low temperature region 200–300 °C as it is expected to be favorable for formation of surface NO_x species and therefore most relevant to understand the H₂-effect in modification of surface NO_x species.

Experimental method

Catalyst preparation

Ag–Al₂O₃ with 2 wt.% Ag loading on Al₂O₃ was prepared by a freeze dried sol-gel method. The powder was then washcoated onto a cordierite monolith with a diameter of 2 cm. Ag–Al₂O₃ and Al₂O₃ were washcoated onto 2 cm and 4 cm long cordierite monoliths respectively. Approximately 0.5 g of Ag–Al₂O₃ and 1.5 g Al₂O₃ was deposited onto the cordierite monoliths. The specific surface area of powders measured by N₂ sorption (BET method) gave specific surface areas of 188 m² g^{−1} and 233 m² g^{−1} for Ag–Al₂O₃ and Al₂O₃, respectively. The details of methods for preparation and coating of monoliths were described elsewhere.^{21,27}

Flow reactor experiments

TPD experiments were performed in a horizontal quartz tube reactor 88 cm long with 2 cm diameter. The monolith sample was placed inside the reactor tube and thermocouples were used to measure both the monolith temperature (later also called catalyst temperature) and inlet gas temperatures. To minimize axial temperature gradients in the monolith sample, a number of blank monoliths (with total length of 14 cm) were placed to fill the empty space between the monolith and outlet end of the reactor. A test with only blank monoliths indicated that these blank monoliths were inert. To provide heat to the reactor, a spiral-shaped electrical heater was used around the reactor tube. A number of quartz wool layers were used to bundle the reactor tube in order to minimize heat loss.

Several mass flow controllers (Bronkhorst) were used to supply gas flow to the reactor tube. Ar was used as a carrier gas in all experiments. The outlet flow from the reactor was sent to gas analyzers. A FTIR MKS 2000 was utilized to measure the majority of gas outlet component concentrations including NO, NO₂, N₂O, CO, C₃H₆, and NH₃ in ppm level. In addition, a Hiden HPR 20 quadrupole mass spectrometer (MS) was employed to sample a small fraction of the outlet stream to detect variations in concentrations of some components from the following mass to charge (*m/z*) ratios: 2 (H₂), 16 and 32 (O₂), 28 (N₂ and CO), and 44 (CO₂). To present O₂ measurement results, *m/z* 16 was selected from MS measurement.

Temperature-programmed desorption experiments (TPD) were initiated by pretreatment of the catalyst with 8% O₂ for 20 minutes at 550 °C. Subsequently, the catalyst temperature was cooled down to a targeted adsorption temperature: 200, 250 or 300 °C. An adsorption gas mixture was introduced for a certain time as depicted in Table 1. After the adsorption



Table 1 Composition of adsorption gases, space velocity and duration of adsorption steps in flow reactor experiments

TPD type	Gas mixture (GM)	Adsorption gases ^a	2 wt.% Ag–Al ₂ O ₃		Al ₂ O ₃	
			Duration (min)	WHSV ^b (h ⁻¹)	Duration (min)	WHSV ^b (h ⁻¹)
NO oxidation	GM 1	500 ppm NO + 4% O ₂	30	266	30	231
H ₂ -assisted NO oxidation	GM 2	500 ppm NO + 4% O ₂ + 0.1% H ₂	30	266	30	231
NO ₂ –O ₂ adsorption	GM 3	150 ppm NO ₂ + 4% O ₂	120	620	180	231
C ₃ H ₆ -SCR	GM 4	500 ppm NO + 0.1% C ₃ H ₆ + 4% O ₂	30	266	—	—
H ₂ -assisted C ₃ H ₆ SCR	GM 5	500 ppm NO + 0.1% C ₃ H ₆ + 4% O ₂ + 0.1% H ₂	30	266	—	—

^a Ar was always used as carrier gas. ^b Weight hourly space velocity (WHSV) is the ratio of mass flow rate and mass of catalyst material.

step, feed of adsorption species were terminated and a flow of only Ar was maintained. The catalyst temperature was then kept constant at the adsorption temperature for 5 minutes to flush away any loosely bound surface species. Subsequently, the catalyst temperature was either maintained or decreased to 200 °C during a period of 30 min in Ar flow to allow further stabilization of the adsorbed species. The desorption step was performed by increasing the inlet gas temperature from 200 to 550 °C at a rate of 40 °C min⁻¹ in Ar flow. Due to temperature gradients between measured inlet and catalyst temperatures, the maximum catalyst temperature reached varied between 530 to 545 °C. The catalyst temperature was the temperature used to identify the desorption profile and is therefore presented in all TPD results below.

During adsorption with C₃H₆-SCR conditions (GM 4 in Table 1), H₂-assisted C₃H₆-SCR (GM 5 in Table 1) as well as the following desorption steps, it was found that formation of N₂O according to the FTIR analysis was negligible. Therefore, *m/z* 44 from MS measurement could be used as a reliable indicator of CO₂ concentration with calibration. These MS measurements of CO₂ concentration agreed quantitatively with average FTIR measurements but were found to be far less noisy and are thus reported here.

Total flow rates of gases during flow reactor experiments were varied between 1500–3500 mLn min⁻¹. As a result, different weight hourly space velocities (WHSV) were used for the Ag–Al₂O₃ and Al₂O₃ catalysts based on the masses of catalyst material deposited on monoliths as shown in Table 1. It is thus noteworthy that the quantities of adsorbed species cannot be compared directly by merely inspecting the level of gas concentrations from TPD results over Ag–Al₂O₃ and Al₂O₃. A lower WHSV was usually used for the Al₂O₃ catalyst because it was expected that the quantities of adsorbed species would be lower compared to Ag–Al₂O₃ and thus there would be a risk that the desorbed

quantities may be undetectable during the TPD experiments. Nevertheless, correct comparisons could be made since the flow reactor experimental results were integrated to calculate the quantities of adsorbed/desorbed NO_x species per mass of catalyst materials.

In situ DRIFT Spectroscopy

The DRIFT instrument used in this work was a Bio Rad FTS6000 Spectrometer. The sample powder of 2 wt.% Ag–Al₂O₃ was placed in a sample holder (supported by a metallic grid) of a high temperature Harrick Praying Mantis cell coated with Silcolloy® 1000 and equipped with KBr windows. The gases were supplied by a number of mass flow controllers (Bronkhorst Hi-Tech). The total flow used was 100 mLn min⁻¹ with Ar as the inert balance. The weight of sample powder was *ca.* 90 mg. To regulate temperature, the DRIFT cell was equipped with a Eurotherm heating system and water cooling system. In addition, a K-type thermocouple was placed near the sample holder to indicate the bed temperature.

The DRIFT experiments were conducted following a similar TPD protocol that consisted of adsorption and desorption steps with temperature ramps. Prior to each experiment, the sample was pretreated with 8% O₂ at 500 °C for 30 min. Subsequently, the cell temperature was decreased to 200 °C in inert gas flow. Here, background spectra were collected prior to each adsorption step by accumulating 60 scans with a resolution of 1 cm⁻¹. The accumulation of IR spectra was initiated 2 min before the adsorption step by collecting 6 scans min⁻¹ with a resolution of 1 cm⁻¹. Table 2 shows the details of the adsorption step conditions. After the adsorption step, the cell temperature was kept constant at 200 °C for 10 min to stabilize adsorbed species in Ar flow. Subsequently, the cell temperature was raised to 500 °C with a ramping rate of

Table 2 Composition of adsorption gases and duration of adsorption steps for *in situ* DRIFT Spectroscopy

No.	Adsorption step	Adsorption gases	Duration (min.)
1	NO oxidation	1000 ppm NO + 8% O ₂	30
2	H ₂ -assisted NO oxidation	1000 ppm NO + 8% O ₂ + 0.2% H ₂	30
3	NO ₂ –O ₂ adsorption	300 ppm NO ₂ + 8% O ₂	60
4	C ₃ H ₆ -SCR	1000 ppm NO + 8% O ₂ + 2000 ppm C ₃ H ₆	30
5	H ₂ -assisted C ₃ H ₆ -SCR	1000 ppm NO + 8% O ₂ + 2000 ppm C ₃ H ₆ + 0.2% H ₂	30



20 °C min⁻¹. The IR spectra were collected continuously during adsorption and desorption steps.

Results

TPD following NO oxidation

In order to investigate formation of surface NO_x species, adsorption conditions with NO–O₂ gas mixture (GM 1) was carried out over Ag–Al₂O₃ and Al₂O₃. Fig. 1 shows the NO_x uptake during the adsorption step and TPD profile over Ag–Al₂O₃ and Al₂O₃. The amount of NO_x adsorbed and desorbed was calculated by integrating the NO_x curves over these catalysts and normalized to the mass of catalyst. The results from integration are displayed in Table 3.

As seen from Fig. 1 and Table 3, the quantities of NO_x adsorbed decreased with increasing adsorption temperature. It was found that the duration of adsorption was in all cases sufficiently long to reach steady state reaction conditions and thus the catalyst was saturated with adsorbed species for each set of conditions. Conversion of NO to NO₂ during

the adsorption step over Ag–Al₂O₃ (Fig. 1a) was low and negligible at 200 and 250 °C. At 300 °C, there was a detectable conversion of NO to NO₂ of about 4%. Following the switch from the adsorption gas mixture to only Ar flow, there was desorption of loosely bound surface NO_x species.

Fig. 1b shows the desorption profiles of NO_x over Ag–Al₂O₃. During the temperature ramp for Ag–Al₂O₃, two NO_x desorption peaks were observed *i.e.* a low temperature (LT) peak at 277–340 °C and high temperature (HT) peak at *ca.* 440 °C. It is noteworthy that the LT peaks were skewed to higher temperatures with increasing adsorption temperature. The major NO_x components desorbed were NO at both LT and HT peaks whereas NO₂ was only observed at the LT peak following adsorption at 200 and 250 °C. No O₂ release was observed during the desorption steps following all adsorption temperatures.

In order to investigate the formation of surface NO_x species over Al₂O₃, similar TPD studies following NO oxidation were conducted on Al₂O₃ (Fig. 1c and d). As seen from Fig. 1c, the NO oxidation conversion to NO₂ was negligible and at the highest temperature 300 °C, only *ca.* 8 ppm of

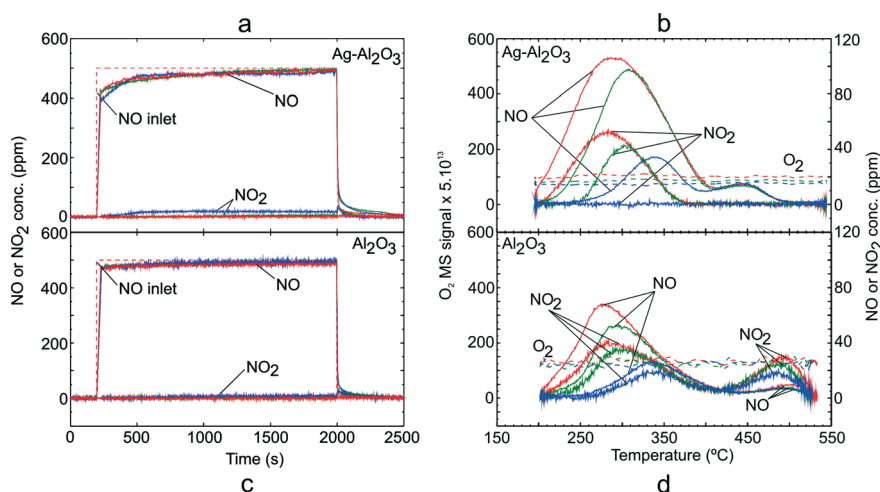


Fig. 1 TPD following NO oxidation over Ag–Al₂O₃ and Al₂O₃ showing the adsorption steps (a, c) and desorption profiles (b, d) at adsorption temperature 200 (red), 250 (green) and 300 °C (blue). Adsorption condition GM 1 as displayed in Table 1 was used.

Table 3 Quantities of NO_x adsorbed and desorbed over Ag–Al₂O₃ and Al₂O₃

Adsorption conditions	Ag–Al ₂ O ₃		Al ₂ O ₃	
	NO _x adsorbed (μmol g ⁻¹)	NO _x desorbed (μmol g ⁻¹)	NO _x adsorbed (μmol g ⁻¹)	NO _x desorbed (μmol g ⁻¹)
TPD NO–O ₂				
200 °C	111.4	110.7	61.9	59.6
250 °C	98.2	98.1	57.9	57.7
300 °C	59.3	58.7	41.5	40.9
TPD NO–O ₂ –H ₂				
200 °C	189.6	188.8	31.3	28.7
250 °C	153.5	150.8	17.8	14.0
300 °C	103.7	100.4	8.8	6.8
TPD NO ₂ –O ₂				
200 °C	450.8	448.9	357.6	356.6
250 °C	337.9	335.4	282.3	281.2
300 °C	245.7	242.4	212.6	210.8



NO₂ (~1.6% conversion) was observed. Thus, it can be said that both Ag–Al₂O₃ and Al₂O₃ could be considered as a relatively poor NO oxidation catalysts below 300 °C. From the desorption profile (Fig. 1d), two desorption peaks were observed, similar to that for the Ag–Al₂O₃ catalyst. The characteristics and location of the LT peak resembled that for Ag–Al₂O₃. However, the HT peak over Al₂O₃ was shifted to a higher temperature of 486 °C. The major gas desorbed at the LT peak was NO followed by a slightly lower amount of NO₂. Whereas, decomposition of surface NO_x species at the HT peak gave mostly NO₂. Similar to Ag–Al₂O₃, no desorption of O₂ was observed during temperature ramps following all adsorption temperatures.

TPD following H₂-assisted NO oxidation

Addition of H₂ has been shown to promote NO oxidation activity over Ag–Al₂O₃ catalysts.^{5,8,13,17,18,20,21} TPD studies using a NO–O₂–H₂ adsorption gas mixture (GM 2) were carried out over Ag–Al₂O₃ and Al₂O₃. Fig. 2 shows the NO_x uptake and TPD profile for the NO–O₂–H₂ system over Ag–Al₂O₃ and Al₂O₃ catalysts. The duration of adsorption was in all cases sufficiently long to reach steady state reaction conditions. As shown in Fig. 2a, NO oxidation conversion to NO₂ was detected and increased from 5% at 200 °C to 10% at 250 and 300 °C during the adsorption step with Ag–Al₂O₃. In addition, formation of N₂O and NH₃ were negligible at below 5 ppm and 1 ppm (not shown), respectively. Likewise, NO_x conversion was not observed.

During the temperature ramp with Ag–Al₂O₃ (Fig. 2b), the desorption peak of NO₂ at ca. 450 °C was clearly observed which can be assigned as the HT peak as observed from NO–O₂ TPD (Fig. 1b). Desorption of O₂ was also observable and coincided well with the NO₂ peak. In addition, desorption of low concentrations of NO were observed at ca. 340–350 °C and 505 °C. It is noteworthy that H₂ desorption was not observed at all temperatures.

It can be noted that along with higher activity for NO oxidation in the presence of H₂, the LT peak which was observed in the NO–O₂ system was significantly suppressed and shifted towards the HT peak. The shift was also accompanied by higher total quantities of NO_x adsorbed and desorbed as displayed in Table 3. The results from the TPD study with Al₂O₃ with adsorption gases GM 2 are shown in Fig. 2c and d. During the adsorption step (Fig. 2c), NO conversion to NO₂ was negligible at all temperatures. Therefore, it could be concluded that H₂ did not promote NO oxidation to NO₂, but instead it acted as a reductant which also decreased the amount of NO_x adsorbed compared to the NO–O₂ system over Al₂O₃ (see Fig. 1c and Table 3).

During the temperature ramp with Al₂O₃ (Fig. 2d), the LT and HT desorption peaks were observable for adsorption temperatures 200 and 250 °C. The LT peak (at 270–280°) was markedly higher than the HT peak (at ca. 460°). The LT peak consisted of NO and NO₂ where the quantities of NO were slightly higher than NO₂. Decomposition of HT species gave only desorption of NO₂. At an adsorption temperature of 300 °C, the desorption peaks of NO_x were at trace levels. In addition, no desorption of O₂ was observed following all studied adsorption temperatures.

TPD following NO₂ adsorption

In order to investigate the adsorption of NO₂ on Ag–Al₂O₃ and Al₂O₃ at conditions comparable to those for NO oxidation above, *i.e.* with excess O₂ present, TPD experiments following exposure to gas mixture GM 3 were conducted. Fig. 3 shows the NO_x uptake and NO_x desorption profiles for both catalysts. As seen from the adsorption step over Ag–Al₂O₃ (Fig. 3a), a temporary formation of NO could be detected during NO₂ adsorption. The quantities of NO_x uptake decreased with higher adsorption temperature as also displayed in Table 3. The NO₂–O₂ system took much longer time to reach stable outlet NO_x signals during the

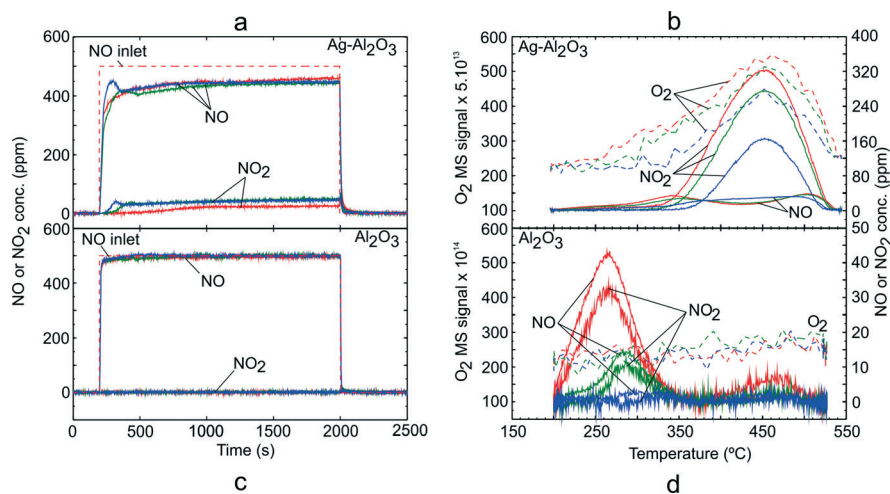


Fig. 2 TPD following H₂-assisted NO oxidation over Ag–Al₂O₃ and Al₂O₃ showing the adsorption steps (a, c) and desorption profiles (b, d) at adsorption temperature 200 (red), 250 (green) and 300 °C (blue). Adsorption condition GM 2 as displayed in Table 1 was used.



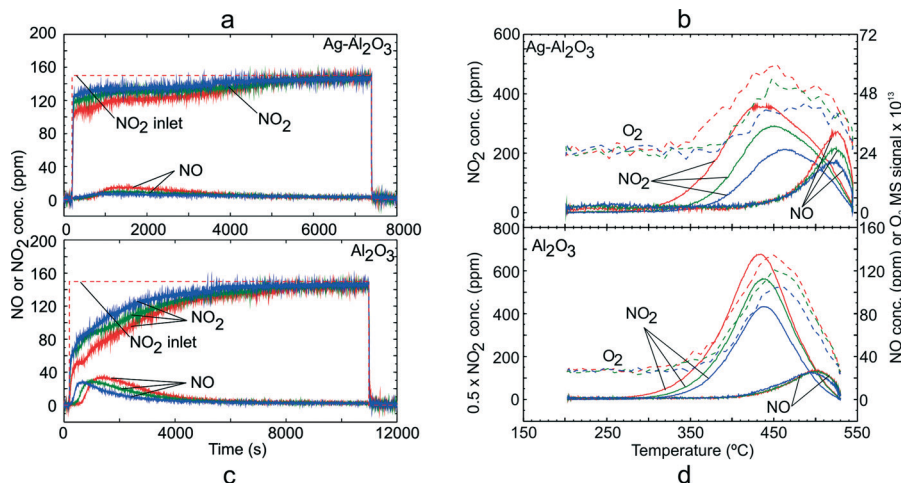


Fig. 3 TPD following NO_2 adsorption over $\text{Ag-Al}_2\text{O}_3$ and Al_2O_3 showing the adsorption steps (a, c) and desorption profiles (b, d) at adsorption temperature 200 (red), 250 (green) and 300 °C (blue). Adsorption condition GM 3 as displayed in Table 1 was used.

adsorption steps compared to the NO-O_2 system due to the larger formation of surface NO_x species on the catalysts as evident from Table 3. During the temperature ramp over $\text{Ag-Al}_2\text{O}_3$ (Fig. 3b), a substantial release of NO_2 was observed that peaked at 440–460 °C. A minor desorption of NO was also detected at higher temperature ~525 °C. A broad release of O_2 was observed reaching a peak at ~450–475 °C.

A similar TPD study with GM 3 was also conducted over the Al_2O_3 sample. Fig. 3c shows the NO_x uptake over the Al_2O_3 catalyst and it gave a profile similar to that for the $\text{Ag-Al}_2\text{O}_3$ catalyst. Along with adsorption of NO_2 , temporary NO formation was also observed and reached a peak of ca. 35 ppm (adsorption temperature 200 °C). Similar to $\text{Ag-Al}_2\text{O}_3$, a broad O_2 peak was observed with a peak at ~450 °C. In general, one can notice that the desorption profiles of NO_x over $\text{Ag-Al}_2\text{O}_3$ and Al_2O_3 after NO_2 adsorption were similar. Comparing the quantities of NO_x , it can be seen from Table 3 that the amount of NO_x adsorbed on $\text{Ag-Al}_2\text{O}_3$ is comparable to Al_2O_3 but somewhat greater on the $\text{Ag-Al}_2\text{O}_3$. It should be

noted that in this case since the WHSV used for $\text{Ag-Al}_2\text{O}_3$ (620 h^{-1}) was much higher than that for Al_2O_3 (231 h^{-1}), the quantities of NO_x adsorbed cannot be compared directly from Fig. 3a and c.

TPD following C_3H_6 -SCR and H_2 -assisted C_3H_6 -SCR

Further TPD studies were conducted to investigate the quantities and nature of adsorbed NO_x and CO_x species during C_3H_6 -SCR and H_2 -assisted C_3H_6 -SCR over the $\text{Ag-Al}_2\text{O}_3$ catalyst. Fig. 4 presents TPD results following exposure to the C_3H_6 -SCR gas mixture (GM 4) in the absence of H_2 where panels 4a to 4d show the NO_x uptake, desorption profile of NO_x , CO_x formation during adsorption and the desorption profile of CO_x respectively.

During the adsorption step (Fig. 4a), the NO signal increased rapidly and NO_2 yield was found to be negligible. Formation of N_2O (not shown) was negligible at below 5 ppm during C_3H_6 -SCR and also later during H_2 -assisted C_3H_6 -SCR.

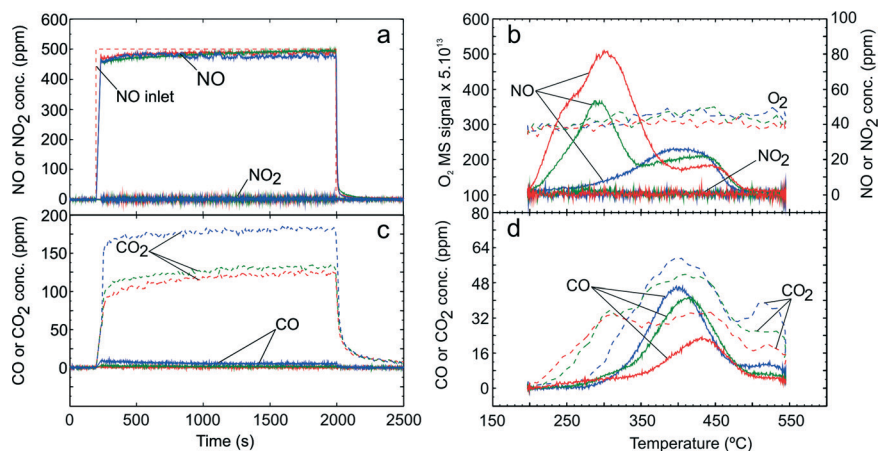


Fig. 4 TPD following C_3H_6 -SCR over $\text{Ag-Al}_2\text{O}_3$ showing adsorption (a) and desorption (b) of NO_x , adsorption (c) and desorption (d) of CO_x . Adsorption condition GM 4 as displayed in Table 1 was used at adsorption temperatures 200 (red), 250 (green) and 300 °C (blue).



Similarly, formation of NH_3 (not shown) was negligible at below 1 ppm both during C_3H_6 -SCR and H_2 -assisted C_3H_6 -SCR. The NO_x conversion during the adsorption step was negligible at less than 250 °C and increased to ~6% at 300 °C. Furthermore, C_3H_6 conversion to CO_2 and CO was also observed during the adsorption step for C_3H_6 -SCR (Fig. 4c).

During the temperature ramp (Fig. 4b), two remarkable NO_x peaks could be observed at ca. 290 °C (LT) and 420 °C (HT). It should be noted that following adsorption at 200 °C a shoulder on the NO peak at ca. 235 °C could be seen. The LT NO_x desorption quantity decreased with higher adsorption temperature and became markedly suppressed at the adsorption temperature of 300 °C. In addition, it could be seen that almost no O_2 desorption was detected during desorption step. From Fig. 4d, the CO desorption peak was observed between 405 to 426 °C while the CO_2 desorption peak was broad with the same rise and decline as the CO profile.

In order to investigate the influence of H_2 on C_3H_6 -SCR, 0.1% H_2 was added in the adsorption step with gas mixture GM 5. Fig. 5a to f showing the NO_x uptake, desorption profile of NO_x , CO_x formation during adsorption, desorption profile of CO_x , H_2 profile during adsorption and desorption profile of H_2 respectively. During the adsorption step (Fig. 5a), NO consumption and NO_2 formation were observed and increased with higher adsorption temperature. An NO_2 yield of up to 20 ppm was observed at adsorption temperature 300 °C. Similarly, higher formation of CO and CO_2 were observed in comparison with the absence of H_2 (comparing Fig. 5c and 4c) indicating a higher conversion of C_3H_6 . Consumption of H_2 during the adsorption step (Fig. 5e)

markedly increased with higher adsorption temperature. As expected, addition of H_2 gave higher NO_x conversion than in the absence of H_2 and a NO_x conversion up to 23% was observed at 300 °C. During the desorption step (Fig. 5b), a small peak of NO at 240 °C and a broad desorption peak reaching a maximum at ~440 °C were observed whereas NO_2 desorption was negligible. These NO peaks decreased with higher adsorption temperature. The quantities of desorbed NO_x in the presence of H_2 were higher than in the absence of H_2 as shown in Table 4. In addition, it could be observed that a broad O_2 desorption was clearly detected accompanying NO_x desorption.

From the desorption profile of CO and CO_2 (Fig. 5d), one can see that a CO peak was observed at ca. 375 °C which is at lower temperature compared to the one in the absence of H_2 . Furthermore, the concentration of CO_x released was much higher than in the absence of H_2 consistent with the higher conversion of C_3H_6 obtained with addition of H_2 . As seen from Fig. 5d and 4d, it can be noted that CO_x desorption does not monotonically decrease with increasing adsorption temperature as was the case with NO_x . Similarly, the desorption profile of H_2 approximately coincided with the CO desorption as shown in Fig. 5f.

Identification and stability of adsorbed surface NO_x species from *in situ* DRIFT

DRIFT spectroscopy was used to investigate types of adsorbed surface NO_x species over $\text{Ag-Al}_2\text{O}_3$. Since the focus was to identify surface NO_x species, only DRIFT spectra within the

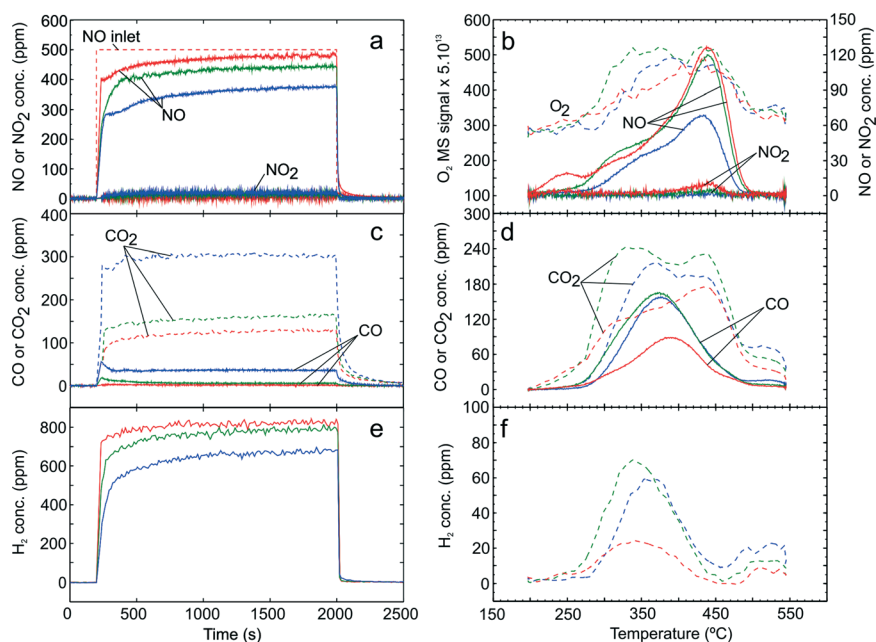


Fig. 5 TPD following H_2 -assisted C_3H_6 -SCR over $\text{Ag-Al}_2\text{O}_3$ showing adsorption (a) and desorption (b) of NO_x , adsorption (c) and desorption (d) of CO_x . Adsorption condition GM 5 as displayed in Table 1 was used at adsorption temperatures 200 (red), 250 (green) and 300 °C (blue).



Table 4 Quantities of NO_x desorbed over Ag–Al₂O₃ after C₃H₆-SCR and H₂-assisted C₃H₆-SCR

Adsorption conditions	C ₃ H ₆ -SCR	H ₂ -assisted C ₃ H ₆ -SCR
	NO _x desorbed (μmol g ⁻¹)	NO _x desorbed (μmol g ⁻¹)
200 °C	70.7	91.4
250 °C	53.5	69.3
300 °C	35.4	50.3

range of 1200–1800 cm⁻¹ are presented. Here, adsorption steps were conducted at 200 °C to obtain a high quantity of NO_x adsorbed species. Fig. 6 shows the evolution of IR spectra ensuing the increase of cell temperature during the desorption steps. Here, the adsorption steps were NO oxidation, H₂-assisted NO oxidation and NO₂-O₂ adsorption (conditions 1–3 respectively in Table 2). As seen from the top panel of Fig. 6 at 200 °C, adsorption of NO–O₂ resulted in the

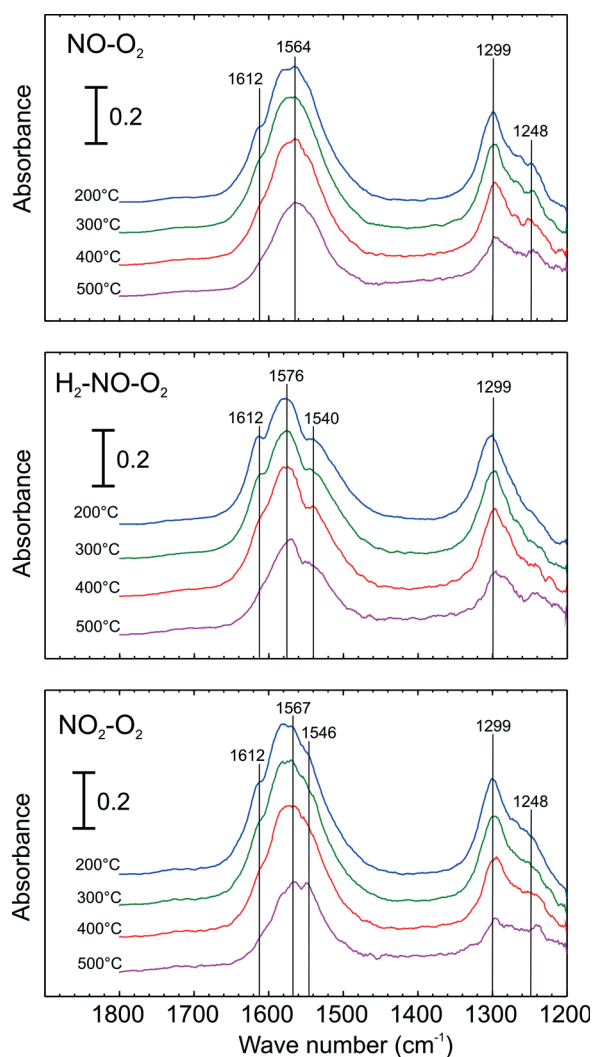
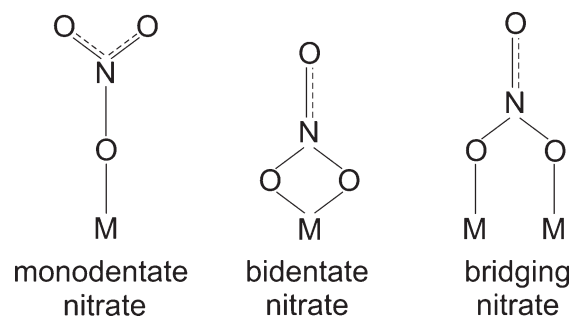


Fig. 6 DRIFT Spectra of adsorbed species during temperature ramp and following adsorption with NO oxidation conditions (top), H₂-assisted NO oxidation conditions (centre) and NO₂-O₂ adsorption (bottom) over 2 wt.% Ag–Al₂O₃ at 200 °C. Adsorption conditions are displayed in Table 2.

appearances of peaks at 1299 and a broad peak at 1564 cm⁻¹. Further, a small peak or shoulder at 1248 and 1612 cm⁻¹ were also seen. When H₂ was added with NO and O₂ (middle panel), several peaks were observed: a notable peak at 1299, a broad peak at 1576 and shoulders at 1612 and 1540 cm⁻¹. It is important to mention that the shoulder peak at 1248 cm⁻¹, clearly evident for the NO–O₂ system, declined in the presence of H₂. When the catalyst was exposed to NO₂-O₂ adsorption (bottom panel), IR spectra with vibration bands at 1248, 1299, shoulder at 1546, a broad peak at ca. 1567 and shoulder at 1612 cm⁻¹ were observed.

Possible structures of adsorbed nitrate species namely monodentate nitrate, bidentate nitrate and bridging nitrate are shown in Scheme 1 and peak assignments were mainly taken from our group's publications.^{24,28} The vibration band at 1248 cm⁻¹ can be assigned to bidentate nitrate as reported in literature.^{10,28} The peak at 1299 is also attributable to bidentate nitrate that was reported by literature at 1298, 1300 and 1304 cm⁻¹.^{28,29} In the higher wavenumber regions (approximately between 1540–1615 cm⁻¹), broad peaks at 1564 and 1576 cm⁻¹ were observed resulting from the overlap of monodentate nitrate (1530–1546, 1558–1564 cm⁻¹)²⁴ and bidentate nitrate (1570–1590 cm⁻¹).²⁴ In addition, the shoulder peaks observed at 1612 cm⁻¹ may be ascribed to the vibration of bridging nitrate that has been reported at 1614 cm⁻¹.^{24,25,28}

In order to investigate the thermal stability of adsorbed NO_x species, the cell temperature was increased to 500 °C in Ar flow. Fig. 6 presents a number of IR spectra at different temperatures during the temperature ramp. As seen here, the intensity of the bridging nitrates (1612 cm⁻¹) readily disappeared in all cases. Further, it can be observed that the subsequent peak that decreased abruptly was that of the bidentate nitrate. The broad peak at 1564 cm⁻¹ (top panel) and 1576 cm⁻¹ (middle and bottom panel) tended to shift to the lower wavenumbers resulting from a decrease in bidentate nitrates, indicating peak separation of bidentate and monodentate nitrates. Comparing the intensity of the monodentate nitrate band (1540 or 1546 cm⁻¹), it is interesting to note that its presence is more prevalent in the case of H₂-assisted NO oxidation (middle panel) and NO₂-O₂ adsorption (bottom panel) compared to the case of NO–O₂



Scheme 1 Possible structures of surface nitrate species (M = metal ion). Adapted from ref. 25 and references therein.



adsorption (top panel). As seen during the temperature increase here, the intensity of monodentate nitrates are apparently the most stable among nitrate species.

Further *in situ* DRIFT experiments were carried out to investigate the stability of adsorbed NO_x species following adsorption with C_3H_6 -SCR and H_2 -assisted C_3H_6 -SCR conditions. Fig. 7 presents the evolution of the DRIFT spectra during the temperature ramp following adsorption with C_3H_6 -SCR and H_2 -assisted C_3H_6 -SCR conditions. As seen from the top panel of Fig. 7 after adsorption from C_3H_6 -SCR (indicated at 200 °C), vibration bands assignable to monodentate nitrate at 1546 cm^{-1} were observed. Strong vibration bands at 1299 and a broad peak at 1584 as well as shoulder at 1248 cm^{-1} , ascribable to bidentate nitrate²⁸ were apparent. A shoulder peak at 1612 cm^{-1} , assignable to bridging nitrate, was also detected as in previous cases. In addition, small bands were observed at 1393 and 1378 cm^{-1} that may be ascribed to formate²⁸ or acetate²⁹ species and thus unrelated to the vibration of surface NO_x species.

When H_2 was added (lower panel of Fig. 7 at 200 °C), similar IR spectra were obtained as in the case of C_3H_6 -SCR adsorption conditions. In comparison to the case of C_3H_6 -SCR conditions, it can be seen that the shoulder peak at 1248 cm^{-1} had lower relative intensity. In contrast, the vibration band at 1546 cm^{-1} had a higher relative intensity. Similar to C_3H_6 -SCR, broad peaks at 1299 and 1588 cm^{-1} ,

assignable to bidentate nitrates, were outstanding. Also a peak at 1612 cm^{-1} , assignable to bridging nitrate, was also observable. Finally, peaks at 1393 and 1379 cm^{-1} were observed with higher intensity for H_2 -assisted C_3H_6 -SCR, attributed to acetate/formate species.

When the cell temperature was increased, as shown in Fig. 7, the bridging nitrates readily disappeared followed by a rapid decrease in bidentate nitrates at both 1588 and 1299 cm^{-1} . At the highest temperature (500 °C), again the vibration band assigned to monodentate nitrate (1546 cm^{-1}) was still observable showing its strong stability at high temperature. It is noticeable that the acetate/formate species also have rather strong stability with temperature (lower panel of Fig. 7), having disappeared finally at 500 °C .

Discussion

Formation of adsorbed NO_x species from NO oxidation

From the results of TPD following NO-O_2 exposure over $\text{Ag-Al}_2\text{O}_3$ and Al_2O_3 , the NO_x desorption profile over both catalysts was similar showing two desorption peaks; one at low temperature referred to as the LT peak (a major peak) and one at high temperature referred to as the HT peak (a minor peak). The increase in NO oxidation conversion with increase in temperature was accompanied by a decrease in the LT NO_x desorption peak. These NO_x desorption peaks, can then be considered to originate from the decomposition of two types of surface NO_x species: a less thermally stable LT surface NO_x species and more stable HT surface NO_x species.

From DRIFT results, the thermal stability of nitrate species were found to be in the order of bridging < bidentate < monodentate nitrate and therefore it is reasonable to regard the LT desorption peak to primarily originate from the decomposition of bidentate and bridging nitrate species, as in accordance with an earlier report.⁶ In the presence of H_2 in the feed, it is apparent that the formation of the bidentate nitrate at 1248 cm^{-1} was less pronounced. This result is in agreement with Shibata *et al.*¹⁰ who reported minimal formation of a similar peak for H_2 -assisted C_3H_8 -SCR. We therefore suggest that the vibration of bidentate nitrate at 1248 cm^{-1} can also be associated with the LT desorption peak.

Klacar *et al.*³⁰ performed Density Functional Theory (DFT) calculations of NO_x adsorption over oxidized silver. They found that adsorption of NO and NO_2 over oxidized silver yielded formation of nitrate species, especially on well-dispersed silver clusters (size of clusters 4–8 atoms) indicating that surface NO_x species borrow O atoms from the Ag to form mainly bridging nitrates. Additionally, similar TPD profiles following NO-O_2 adsorption were observed for $\text{Ag-Al}_2\text{O}_3$ and Al_2O_3 and hence a part of these surface NO_x species were also on Al_2O_3 . A similar phenomenon of surface nitrate formation by loaning O atoms over Al_2O_3 can also be speculated, as has been shown by Zhang *et al.*²⁵ As seen from Fig. 1b and d, when the temperature was increased, the LT peak consisted of more NO than NO_2 and it was not accompanied by O_2 desorption. This observed ratio of desorbed

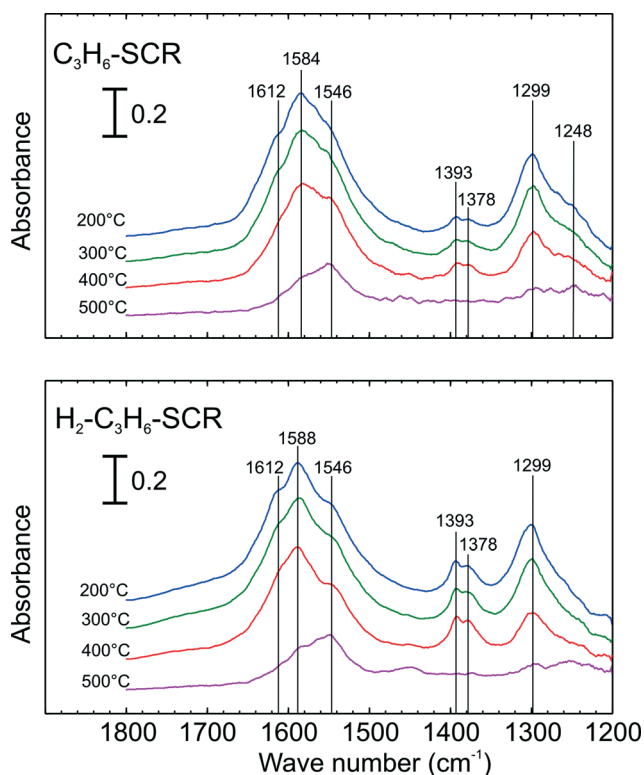


Fig. 7 DRIFT Spectra of adsorbed species during temperature ramp and following adsorption with C_3H_6 -SCR (top) and H_2 -assisted C_3H_6 -SCR conditions (bottom) over 2 wt.% $\text{Ag-Al}_2\text{O}_3$ at 200 °C . Adsorption conditions are displayed in Table 2.



atomic nitrogen to oxygen indicates that the decomposition of nitrate species giving the LT peak should leave borrowed O atoms on Ag and Al_2O_3 .

The HT desorption peak has often been proposed to result from the decomposition of monodentate nitrates that gave desorption of NO , NO_2 and O_2 .^{6,23,25} Here, only a small HT desorption peak was observed that gave mainly NO without O_2 desorption after NO-O_2 exposure. In this case the amount of monodentate nitrate species was likely too small in our monolithic sample to yield detectable O_2 desorption or they also partially left borrowed O atoms on the catalyst surface.

From TPD results for gas mixture of $\text{NO-O}_2\text{-H}_2$ over $\text{Ag-Al}_2\text{O}_3$ (Fig. 2b), it can be noted that along with higher activity for NO oxidation in the presence of H_2 , the LT peak observed in NO-O_2 TPD (Fig. 1b) was significantly suppressed and shifted towards the HT peak (Fig. 2b). However, in the case of Al_2O_3 relatively little suppression in the LT peak was observed (Fig. 2d) along with no promotion of NO oxidation.

Due to the fact that the LT peak decomposed thermally at higher adsorption temperatures and was suppressed significantly in the presence of H_2 which both gave higher NO oxidation conversion, it is therefore reasonable to consider the LT peak to result from the decomposition of surface NO_x species on the active sites. This also tends to indicate that Ag is needed to activate H_2 to suppress formation of surface NO_x species that produce the LT peak. In addition, the active sites in the case of the $\text{Ag-Al}_2\text{O}_3$ catalyst may involve Ag in close vicinity with Al_2O_3 as assumed by others.^{14,31} By associating TPD and DRIFT, we suggest that H_2 eliminated surface nitrate species on active sites (LT peak) which is predominantly bidentate nitrate (1248 cm^{-1}). Our result coincides with that of Chansai *et al.*¹⁴ who used short time exposure (less than 120 s) in DRIFTS-MS study and suggested that the peak at 1255 cm^{-1} assigned as monodentate nitrate in their work was the surface nitrate species located on the active part of the catalyst.

Further, the difference between the integrated LT NO_x ($\text{NO} + \text{NO}_2$) peaks from Fig. 1b (over $\text{Ag-Al}_2\text{O}_3$) and d (over Al_2O_3) can give an indication of the coverage of surface NO_x species on active Ag sites. Fig. 8a displays these results from TPD after NO-O_2 exposure between 200 and 300 °C over both catalysts. As shown here, the coverage of surface NO_x species on Ag sites decreased with higher temperature. By comparing with the amount of Ag available in the catalyst, the estimated amount of LT NO_x on active sites (difference between $\text{Ag-Al}_2\text{O}_3$ and Al_2O_3) is much lower than the total amount of Ag ($148\text{ }\mu\text{mol g}^{-1}$). At 200 and 250 °C, this LT NO_x corresponded to 18% and 14% respectively of the total Ag, indicating that the dispersion of active sites may be comparable to these values.

At 300 °C, it could be observed that the amount of surface NO_x species on $\text{Ag-Al}_2\text{O}_3$ was more or less equal to Al_2O_3 , thereby indicating that Ag sites were largely free from LT surface NO_x species by 300 °C. The differences in surface area for the $\text{Ag-Al}_2\text{O}_3$ ($188\text{ m}^2\text{ g}^{-1}$) and Al_2O_3 ($233\text{ m}^2\text{ g}^{-1}$)

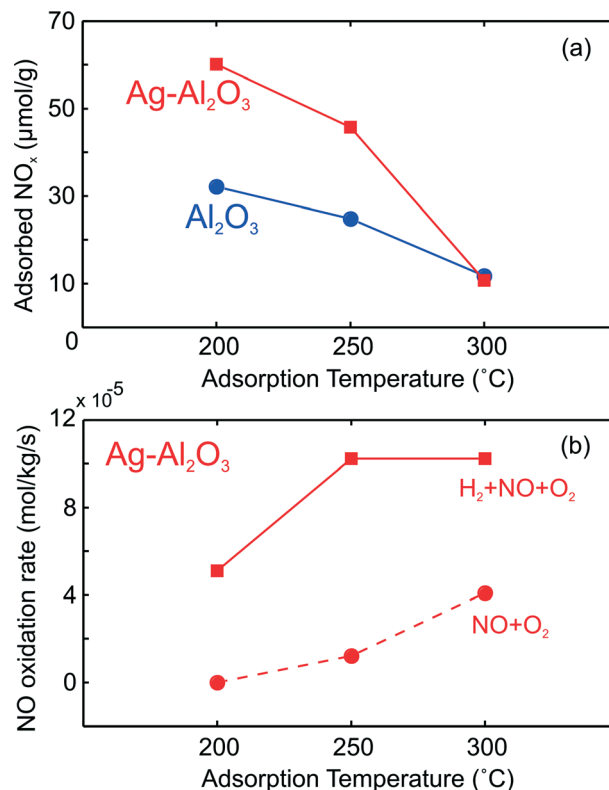


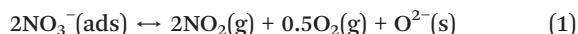
Fig. 8 The amount of surface NO_x species from integration of LT desorption peak after NO-O_2 adsorption over $\text{Ag-Al}_2\text{O}_3$ and Al_2O_3 as shown earlier in Fig. 1 (upper panel, a) and reaction rate for NO oxidation and H_2 -assisted NO oxidation over $\text{Ag-Al}_2\text{O}_3$ (lower panel, b).

samples suggest that differences in their LT NO_x adsorption cannot exactly quantify the NO_x on Ag sites. However even disregarding NO_x adsorption on Al_2O_3 , it is clear that at least 80% of Ag sites were freed from LT surface NO_x species by 300 °C compared to 200 °C. Fig. 8b compares the calculated reaction rates for NO oxidation (Fig. 1a) and H_2 -assisted NO oxidation (Fig. 2a). As seen here, the rate of NO_2 formation was always higher in the presence of H_2 at all temperatures, even at 300 °C where Ag was largely free from the presumably inhibiting LT NO_x species. If removal of inhibiting nitrate species was the only promoting role of H_2 for NO oxidation, one would expect the NO oxidation reaction rates with and without H_2 feed to be nearly equal at 300 °C. If all inhibiting surface NO_x species were thermally removed at 300 °C, comparison of reaction rates at this temperature indicates that as much as 60% of total rate with H_2 feed could not be due to removal of inhibiting surface NO_x . Therefore, this points out that H_2 should have additional promoting roles.

As shown in Fig. 2b, the shift of the NO_x desorption peak upon introduction of H_2 over $\text{Ag-Al}_2\text{O}_3$ was also accompanied by higher total quantities of NO_x adsorbed and desorbed (Table 3) which was not observed for the case of Al_2O_3 . H_2 induced NO_x adsorption over $\text{Ag-Al}_2\text{O}_3$ can then be related to the increase of the HT surface NO_x species. Surface decomposition of the HT surface NO_x species resulted in the release of



NO₂ and O₂ and can be explained by eqn (1) as has been addressed by Guo *et al.*⁷



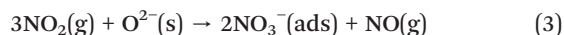
The mechanistic role of H₂ to promote NO_x adsorption will be discussed further after following section.

TPD studies following NO₂–O₂ adsorption

The quantity and types of surface NO_x species formed is also related to the NO_x species composition of the gas phase and therefore TPD studies following NO₂–O₂ adsorption were conducted. As seen from the DRIFT results in the lower panel of Fig. 6, formation of various surface nitrate species were detected upon exposure to NO₂ and O₂. From Fig. 3a and c, formation of NO was observable during the NO₂–O₂ adsorption over Ag–Al₂O₃ and Al₂O₃. By integration of the curves in Fig. 3a and c, the average ratio of total NO₂ uptake to total NO yield was 2.62 for Ag–Al₂O₃ and 3 for Al₂O₃. Therefore, one can deduce that self-oxidation of NO₂ was likely to dominate during the adsorption step according to the following overall reaction:



However, surface oxides may also be involved by donating an O atom/ion similar to that discussed earlier in the first section of discussion part by the following overall reaction:⁷



As seen from reactions (2) and (3), the ratio of NO₂ adsorbed and NO released is 2 in reactions (2) and (3) in reaction (3). The ratios from the integration results fit well and suggest that both reactions are likely occurring during NO₂–O₂ adsorption, with the reaction involving surface oxides as in reaction (3) being most dominant for Al₂O₃.

During the temperature ramp (Fig. 3b and d), it is interesting to note that TPD after NO₂–O₂ adsorption over both Ag–Al₂O₃ and Al₂O₃ gave broad peaks of NO₂ at temperatures exceeding 430 °C, suggesting that NO₂ favors formation of HT surface NO_x species. As seen from Fig. 3b and d, decomposition of the HT surface NO_x species primarily produced NO₂ and O₂ as described in eqn (1) over a range of temperatures from 350 to 545 °C. The release of NO at more elevated temperatures above 500 °C is probably related to a more extensive decomposition of the surface nitrates or even subsequent decomposition of the released NO₂ that is favored by thermodynamics. Both of these processes would also release gas phase O₂.

The role of H₂ to modify surface NO_x species

TPD results for NO–O₂–H₂ (Fig. 2b) and NO₂–O₂ (Fig. 3b) were similar, giving a substantial release of NO₂ and O₂ at a similar temperature range of the HT peaks. During

adsorption of NO–O₂–H₂ (Fig. 2a), production of NO₂ was always observable. From comparison with Fig. 1b and the low production of NO₂ during NO–O₂ adsorption, it is apparent that NO₂ production is linked to formation of the HT surface NO_x species. Furthermore, additional experiments for NO₂–O₂ TPD on Al₂O₃ (Fig. 3d) gave a similar TPD profile for the same adsorption conditions with Ag–Al₂O₃ (Fig. 3b), suggesting that most of the HT surface NO_x species formed are located on the Al₂O₃ support. Therefore, it was evident that the HT surface NO_x species result from NO₂ adsorption and primarily located on the Al₂O₃ support. It is also then likely that the HT surface NO_x species formed on the Al₂O₃ support are spectator surface species. As has been addressed earlier, these HT surface NO_x species appear to be predominantly in the form of monodentate nitrates by associating the DRIFT and TPD results. These findings agree well with those of Tamm *et al.*²⁴ who suggested one role of H₂ was to facilitate formation of monodentate nitrate that is not poisonous and likely to be located on Al₂O₃.

A mechanism of NO_x storage by a spillover mechanism has been proposed.^{8,11,24} An alternative mechanism of NO_x storage by NO₂ readsorption on the Al₂O₃ support has also been proposed by Johnson II *et al.*³¹ Based on the results of these TPD studies, it is indicative that the NO₂ readsorption mechanism is most probable for NO_x storage on Al₂O₃, since formation of the HT surface NO_x species was related to the presence of gas phase NO₂. However, this does not negate the possibility that a spillover mechanism also contributes to NO_x storage on Ag–Al₂O₃.

As described earlier for NO–O₂–H₂ TPD over Al₂O₃ (Fig. 2d), it is likely that the characteristics of the adsorbed surface NO_x species are not the same over Ag–Al₂O₃ and Al₂O₃. Consequently, desorption of O₂ which was observed over Ag–Al₂O₃ (Fig. 2b) was not observed over Al₂O₃ (Fig. 2d) and NO_x storage during adsorption of NO–O₂–H₂ over Al₂O₃ does not include formation of gas phase NO₂.

Mechanistic insights regarding C₃H₆–SCR and H₂–assisted C₃H₆–SCR

TPD studies with C₃H₆–SCR and H₂–assisted C₃H₆–SCR adsorption conditions were conducted over Ag–Al₂O₃ to study how surface NO_x species affect the NO_x reduction performance. Reaction of surface NO_x species with partially oxidized C₃H₆ is considered as an important step to obtain high activity for C₃H₆–SCR over a Ag–Al₂O₃ catalyst.^{7,32,33}

It is interesting to note that by comparing the NO_x desorption profile in C₃H₆–SCR (Fig. 4b) and NO oxidation (Fig. 1b), both of them have a similar profile with LT and HT NO_x desorption peaks. However, for C₃H₆–SCR (Fig. 5b) the NO₂ desorption is very low probably due to the presence of adsorbed HC species that reduce the surface NO_x species to NO during their decomposition and desorption. This presence of both LT and HT surface NO_x species in approximately the same temperature ranges indicates



that NO oxidation and C₃H₆-SCR should share some mechanistic features.

During the adsorption with C₃H₆-SCR conditions (Fig. 4a), NO_x conversion at 300 °C were clearly higher than 200 and 250 °C. In addition, CO_x desorption was observed during the temperature ramp (Fig. 4d) due to decomposition and oxidation of adsorbed and oxidized HC species. There tended to be more of these species at 300 °C along with greater NO_x reduction activity, suggesting that they are important intermediate species. Removal of the LT inhibiting surface NO_x species at higher temperature (Fig. 4b) likely contributed to more formation of these intermediate species for the NO_x reduction process.⁷

During the adsorption step for H₂-assisted C₃H₆-SCR (Fig. 5a), higher NO_x reduction activity was observed, reaching up to ~23% at 300 °C. The improvement in NO_x reduction activity was also accompanied by a significant decrease in the LT NO_x desorption peak as can be seen by comparing Fig. 5b and 4b. At the same time, the HT NO_x desorption peak increased remarkably. Therefore, again removal of the inhibiting LT surface NO_x species, in this case aided by reaction with H₂, coincided with the improved NO_x reduction activity. Unlike in the case of NO–O₂–H₂ (Fig. 2b) and NO₂–O₂ (Fig. 3b) TPD, the increase of the HT peak for H₂-assisted C₃H₆-SCR (Fig. 5b) gave mostly NO desorption. Additionally, the O₂ desorption, however, was observed during desorption in all cases of TPD for NO–O₂–H₂, NO₂–O₂ and H₂-assisted C₃H₆-SCR. The larger production of NO for H₂-assisted C₃H₆-SCR, probably resulted from the adsorbed HC which was oxidized by the adsorbed NO_x species during their decomposition and desorption. From Fig. 5b, it can also be seen that the HT NO_x desorption peak had a broad shoulder towards lower temperatures. This shoulder probably results from the presence of adsorbed HC species acting as reductants and destabilizing the nitrate species to cause some lower temperature NO_x decomposition.

As seen from comparing Fig. 4d and 5d, the higher concentration of desorbed CO and CO₂ infers that H₂ had a promotional effect on low temperature C₃H₆ activation. Hydrocarbon (HC) activation to form oxidized HC species itself is often suggested as a key step in HC-SCR over Ag–Al₂O₃.^{10,13,16} Greater formation of surface HC and oxidized HC in the presence of H₂ can be linked to the removal of inhibiting surface NO_x species as suggested by the suppression of the LT surface NO_x species also with H₂. There was also a broadening of the CO_x desorption peaks and a shift to lower desorption temperature with the addition of H₂ (comparing Fig. 5d and 4d) which suggests that a greater variety and possibly more reactive adsorbed hydrocarbon species with lower thermal stabilities were formed. This finding again points to the fact that H₂ may have other effects to promote the NO_x reduction activity similar to the case for NO oxidation. The reaction rates for NO_x conversion were 6.1×10^{-5} and 22.5×10^{-5} mol kg⁻¹ s⁻¹ at 300 °C for C₃H₆-SCR and H₂-assisted C₃H₆-SCR, respectively. It seems apparent from Fig. 4b that a large part of the inhibiting LT

NO_x species was removed by 300 °C. Thus, again like that for NO oxidation as much as 73% of the C₃H₆-SCR activity from co-feeding H₂ could not be related to removal of inhibiting LT surface NO_x species.

The amount of CO_x desorbed did not monotonically decrease with higher temperature (Fig. 4d and 5d) as was always the case for adsorbed NO_x species. Greater accumulation of adsorbed species producing CO_x at higher temperature indicates that the reactions activating the HC to form oxygenated HC on the surface have relatively high activation energies. In other words, the activation energy to partially oxidize HC to form oxygenated HC surface species is higher than the activation energies of subsequent reactions between surface NO_x species with the oxygenated HC species that leads to formation of N₂. Greater accumulation of oxygenated HC surface species may also be due to less inhibiting nitrates covering the active sites where oxygenated HC are formed.

As seen from DRIFT results in Fig. 7, nitrate peaks assignable to monodentate, bidentate and bridging nitrates were detected for both C₃H₆-SCR and H₂-assisted C₃H₆ similar to the case with NO_x adsorption (Fig. 6). By increasing temperature, the stability of monodentate nitrate (1546 cm⁻¹) was clearly observed. Comparing the decreasing intensity of bidentate nitrate peaks for C₃H₆-SCR and H₂-assisted C₃H₆-SCR, it was found that the rate of decrease with temperature is somewhat slower for the lower panel of Fig. 7 (H₂-assisted C₃H₆-SCR), indicating that the surface NO_x species here were more stable which is in agreement with the TPD results. Further, it was also found that the relative intensity of formate/acetate bands was higher for the H₂-assisted case which agrees with the TPD observations (Fig. 4d and 5d) that larger quantities of adsorbed HC species are present under the H₂-assisted reaction conditions.

In this series of studies, it seems that the promoting role of H₂ appears to be only partially due to the removal of inhibiting surface NO_x species. As a result the findings here support the possibility of other H₂ promoting roles as already described in the literature.^{5,10,12,13,16,22,23} It has however been observed here that the formation of surface nitrate species in the absence of H₂ depends on the donation of oxygen from surface oxides. As a result the removal or prevented formation of these nitrate species caused by H₂ may be linked to some partial reduction of Ag species and thus formation of sites with enhanced activity. However an investigation of the merits of all other possible roles for H₂ to promote NO oxidation or NO_x reduction is beyond the scope of this study and the methods used here.

Conclusions

A series of TPD experiments have been conducted to investigate formation and stability of surface NO_x species related to the promotional effect of H₂ for NO oxidation and C₃H₆-SCR. Formation of two general groups of surface NO_x species were found to be present: a less thermally stable group of so called



“LT surface NO_x species” and a more thermally stable group of “HT surface NO_x species”. The following conclusions can be drawn from this study.

- The LT NO_x desorption peak observed in this study could be attributed to the decomposition of surface NO_x species formed on the active sites. It was apparent that Ag sites were largely free from these surface NO_x species at and above 300 °C. Elimination or decrease in quantities of these LT surface NO_x species either thermally or by reaction with H₂ correlated with higher NO oxidation and NO_x reduction conversion. However, as much as 60% and 73% of the activity for NO oxidation and NO_x reduction respectively by co-feeding H₂ could not be related to removal of LT NO_x surface species.

- The HT NO_x desorption peak primarily corresponded to the decomposition of surface NO_x species on the Al₂O₃ support. Since the increase of surface NO_x species formed on the Al₂O₃ did not hinder NO oxidation and NO_x reduction, the HT surface NO_x species were mainly comprised of spectator surface species in the form of monodentate nitrates.

- H₂ facilitated formation of surface NO_x species on the Al₂O₃ support. It was indicative that the mechanism of NO_x storage on the Al₂O₃ support was *via* NO₂ readsorption, but spillover may also play a role.

- H₂ facilitated formation of oxygenated HC on the surface that may be aided by removal of inhibiting surface NO_x species on active sites.

- Formation of the LT surface nitrate species depended on the donation of oxygen from surface oxides. As a result the removal or prevented formation of these nitrate species caused by H₂ may entail some partial reduction of Ag species and be linked to enhanced C₃H₆-SCR and NO oxidation activity.

From this study, it was seen that the quantities of surface NO_x species removed from the active sites were small compared to the amount simultaneously stored as spectator species mainly on the alumina support. Therefore, the dual role of H₂ to both eliminate inhibiting surface NO_x species from active sites and promote NO_x storage was elucidated.

Acknowledgements

This work has been financially supported by the Swedish Research Council with grant number 621-2011-3926 and partly within the Competence Centre for Catalysis, which is hosted by Chalmers University of Technology and financially supported by the Swedish Energy Agency and the member companies AB Volvo, ECAPS AB, Haldor Topsøe A/S, Scania CV AB, Volvo Car Corporation AB and Wärtsilä Finland Oy. MMA acknowledged Fredrik Gunnarsson for collaboration in preparing Ag–Al₂O₃ catalyst.

Notes and references

- 1 T. Miyadera, *Appl. Catal., B*, 1993, 2–3, 199–205.

- 2 K.-I. Shimizu and A. Satsuma, *Phys. Chem. Chem. Phys.*, 2006, 8, 2677–2695.
- 3 E. Seker, J. Cavataio, E. Gulari, P. Lorphongpaiboon and S. Osuwan, *Appl. Catal., A*, 1999, 183, 121–134.
- 4 M. Yamaguchi, I. Goto, Z. M. Wang and M. Kumagai, *Stud. Surf. Sci. Catal.*, 1999, 121, 371–374.
- 5 S. Satokawa, J. Shibata, K.-I. Shimizu, A. Satsuma and T. Hattori, *Appl. Catal., B*, 2003, 42, 179–186.
- 6 S. Kameoka, Y. Ukisu and T. Miyadera, *Phys. Chem. Chem. Phys.*, 2000, 2, 367–372.
- 7 Y. Guo, M. Sakurai and H. Kameyama, *Appl. Catal., B*, 2008, 79, 382–393.
- 8 N. Sadokhina, D. Doronkin, P. Pributkov, V. Bukhtiyarov, R. Kvon and A. Stakheev, *Top. Catal.*, 2011, 54, 1190–1196.
- 9 X. She and M. Flytzani-Stephanopoulos, *J. Catal.*, 2006, 237, 79–93.
- 10 J. Shibata, K.-I. Shimizu, S. Satokawa, A. Satsuma and T. Hattori, *Phys. Chem. Chem. Phys.*, 2003, 5, 2154–2160.
- 11 R. Brosius, K. Arve, M. H. Groothaert and J. A. Martens, *J. Catal.*, 2005, 231, 344–353.
- 12 J. P. Breen, R. Burch, C. Hardacre, C. J. Hill and C. Rioche, *J. Catal.*, 2007, 246, 1–9.
- 13 Y. Guo, J. Chen and H. Kameyama, *Appl. Catal., A*, 2011, 397, 163–170.
- 14 S. Chansai, R. Burch and C. Hardacre, *J. Catal.*, 2012, 295, 223–231.
- 15 N. A. Sadokhina, D. E. Doronkin, G. N. Baeva, S. Dahl and A. Y. Stakheev, *Top. Catal.*, 2013, 56, 737–744.
- 16 J. P. Breen and R. Burch, *Top. Catal.*, 2006, 39, 53–58.
- 17 P. Sazama, L. Capek, H. Drobna, Z. Sobalik, J. Dedecek, K. Arve and B. Wichterlova, *J. Catal.*, 2005, 232, 302–317.
- 18 S. T. Korhonen, A. M. Beale, M. A. Newton and B. M. Weckhuysen, *J. Phys. Chem. C*, 2011, 115, 885–896.
- 19 U. Bentrup, M. Richter and R. Fricke, *Appl. Catal., B*, 2005, 55, 213–220.
- 20 R. Burch, J. P. Breen, C. J. Hill, B. Krutzsch, B. Konrad, E. Jobson, L. Cider, K. Eränen, F. Klingstedt and L. E. Lindfors, *Top. Catal.*, 2004, 30–31, 19–25.
- 21 M. M. Azis, H. Härelind and D. Creaser, *Chem. Eng. J.*, 2013, 221, 382–397.
- 22 K.-I. Shimizu, K. Sawabe and A. Satsuma, *Catal. Sci. Technol.*, 2011, 1, 331–341.
- 23 P. S. Kim, M. K. Kim, B. K. Cho, I. S. Nam and S. H. Oh, *J. Catal.*, 2013, 301, 65–76.
- 24 S. Tamm, N. Vallim, M. Skoglundh and L. Olsson, *J. Catal.*, 2013, 307, 153–161.
- 25 X. Zhang, H. He, H. Gao and Y. Yu, *Spectrochim. Acta, Part A*, 2008, 71, 1446–1451.
- 26 F. C. Meunier, J. P. Breen, V. Zuzaniuk, M. Olsson and J. R. H. Ross, *J. Catal.*, 1999, 187, 493–505.
- 27 H. Kannisto, H. H. Ingelsten and M. Skoglundh, *J. Mol. Catal. A: Chem.*, 2009, 302, 86–96.
- 28 H. Härelind, F. Gunnarsson, S. M. S. Vaghefi, M. Skoglundh and P. A. Carlsson, *ACS Catal.*, 2012, 2, 1615–1623.
- 29 X. L. Zhang, Y. B. Yu and H. He, *Appl. Catal., B*, 2007, 76, 241–247.



- 30 S. Klacar, A. Hellman, I. Panas and H. Grönbeck, *J. Phys. Chem. C*, 2010, **114**, 12610–12617.
- 31 W. L. Johnson II, G. B. Fisher and T. J. Toops, *Catal. Today*, 2012, **184**, 166–177.
- 32 T. Furusawa, L. Lefferts, K. Seshan and K. Aika, *Appl. Catal., B*, 2003, **42**, 25–34.
- 33 Y. Yu, X. Zhang and H. He, *Appl. Catal., B*, 2007, **75**, 298–302.

